Current LWIR HSI Remote Sensing Activities at Defence R&D Canada – Valcartier

E. Puckrin, J.-M Thériault, C.S. Turcotte, H. Lavoie, and F. Bouffard
CBRNE Threat Detection Group
Spectral and Geospatial Exploitation Section
DRDC Valcartier
Quebec, QC, Canada

ABSTRACT

Recently, DRDC Valcartier has been investigating longwave hyperspectral imaging (HSI) remote sensing techniques using ground-based and airborne sensors. Specific projects to date involve the development of a new ground-based sensor called MoDDIFS (Multi-Option Differential Detection and Imaging Fourier Spectrometer), and the testing of a commercial-off-the-shelf airborne sensor, called Hyper-Cam-LW.

The MODDIFS project involves the development of a leading edge infrared (IR) hyperspectral sensor optimized for the standoff detection of explosive vapours and precursors. The development of the MoDDIFS HSI sensor is based on the integration of two innovative and successful technologies: (1) the differential Fourier-transform infrared (FTIR) radiometry technology found in the Compact Atmospheric Sounding Interferometer (CATSI) sensor previously developed at DRDC Valcartier, and (2) the hyperspectral imaging technology developed by Telops Inc. The new MoDDIFS sensor will essentially offer the optical subtraction capability of the CATSI system but at high-spatial resolution using an MCT focal plane array of 84×84 pixels. The new MoDDIFS sensor will also offer the potential of simultaneously measuring differential linear polarizations to further reduce the clutter in the measured radiance.

The airborne Hyper-Cam initiative seeks to test the commercially available ground-based Hyper-Cam system, developed by Telops Inc, on a stabilized airborne platform with integrated image motion compensation capability. The Hyper-Cam is also based on the Fourier-transform technology yielding high spectral resolution and enabling high accuracy radiometric calibration. It provides passive signature measurements capability, with up to 320×256 pixels at spectral resolutions of up to 0.25 cm^{-1}. To our knowledge, the Hyper-Cam is the first commercial airborne hyperspectral imaging sensor based on Fourier-transform infrared technology. Airborne measurements and some preliminary performance criteria for the Hyper-Cam are presented in this paper.

PART 1: GROUND-BASED REMOTE SENSING ACTIVITY

1.1 Passive Standoff Differential Detection and CATSI

The Compact ATmospheric Sounding Interferometer (CATSI) [1,2] is a passive infrared system designed for the standoff detection of chemical vapours. Its differential detection capability (U.S. patent) provides two unique features for a field-deployable instrument. First, CATSI, as shown in Fig. 1, maintains a constant calibration, thereby providing reliable quantitative measurements over a long period of time.

Report Documentation Page

Form Approved
OMB No. 0704-0188

1. REPORT DATE	2. REPORT TYPE	3. DATES COVERED
OCT 2009	**N/A**	**-**

4. TITLE AND SUBTITLE	5a. CONTRACT NUMBER
Current LWIR HSI Remote Sensing Activities at Defence R&D Canada ¡V Valcartier	5b. GRANT NUMBER
	5c. PROGRAM ELEMENT NUMBER
6. AUTHOR(S)	5d. PROJECT NUMBER
	5e. TASK NUMBER
	5f. WORK UNIT NUMBER
7. PERFORMING ORGANIZATION NAME(S) AND ADDRESS(ES) **CBRNE Threat Detection Group Spectral and Geospatial Exploitation Section DRDC Valcartier Quebec, QC, Canada**	8. PERFORMING ORGANIZATION REPORT NUMBER
9. SPONSORING/MONITORING AGENCY NAME(S) AND ADDRESS(ES)	10. SPONSOR/MONITOR'S ACRONYM(S)
	11. SPONSOR/MONITOR'S REPORT NUMBER(S)

12. DISTRIBUTION/AVAILABILITY STATEMENT
Approved for public release, distribution unlimited

13. SUPPLEMENTARY NOTES
See also ADB381583. RTO-MP-SET-151 Thermal Hyperspectral Imagery (Imagerie hyperspectrale thermique). Meeting Proceedings of Sensors and Electronics Panel (SET) Specialists Meeting held at the Belgian Royal Military Academy, Brussels, Belgium on 26-27 October 2009., The original document contains color images.

14. ABSTRACT

Recently, DRDC Valcartier has been investigating longwave hyperspectral imaging (HSI) remote sensing techniques using ground-based and airborne sensors. Specific projects to date involve the development of a new ground-based sensor called MoDDIFS (Multi-Option Differential Detection and Imaging Fourier Spectrometer), and the testing of a commercial-off-the-shelf airborne sensor, called Hyper-Cam-LW. The MODDIFS project involves the development of a leading edge infrared (IR) hyperspectral sensor optimized for the standoff detection of explosive vapours and precursors. The development of the MoDDIFS HSI sensor is based on the integration of two innovative and successful technologies: (1) the differential Fourier-transform infrared (FTIR) radiometry technology found in the Compact Atmospheric Sounding Interferometer (CATSI) sensor previously developed at DRDC Valcartier, and (2) the hyperspectral imaging technology developed by Telops Inc. The new MoDDIFS sensor will essentially offer the optical subtraction capability of the CATSI system but at high-spatial resolution using an MCT focal plane array of 84e84 pixels. The new MoDDIFS sensor will also offer the potential of simultaneously measuring differential linear polarizations to further reduce the clutter in the measured radiance. The airborne Hyper-Cam initiative seeks to test the commercially available ground-based Hyper-Cam system, developed by Telops Inc, on a stabilized airborne platform with integrated image motion compensation capability. The Hyper-Cam is also based on the Fourier-transform technology yielding high spectral resolution and enabling high accuracy radiometric calibration. It provides passive signature measurements capability, with up to 320e256 pixels at spectral resolutions of up to 0.25 cm-1. To our knowledge, the Hyper-Cam is the first commercial airborne hyperspectral imaging sensor based on Fourier-transform infrared technology. Airborne measurements and some preliminary performance criteria for the Hyper-Cam are presented in this paper.

15. SUBJECT TERMS

16. SECURITY CLASSIFICATION OF:			17. LIMITATION OF ABSTRACT	18. NUMBER OF PAGES	19a. NAME OF RESPONSIBLE PERSON
a. REPORT	b. ABSTRACT	c. THIS PAGE			
unclassified	**unclassified**	**unclassified**	**SAR**	**14**	

Secondly, it can perform the real-time optical subtraction of the background signal from the target signal without the need for extensive calculations. Supported by unique acquisition software (GASEM) [3], CATSI is capable of on-line chemical vapour identification based on the spectral emission signatures of gases measured in the infrared region from 7 to14 µm. CATSI is a tripod-mounted portable instrument (40 kg), with a single FOV detector (9 mrad) and a full pointing capability.

Current methods for the passive standoff detection of chemical vapors by FTIR spectrometry are often limited by the large clutter IR emission from the intervening atmosphere and background. In order to mitigate the clutter impact and reduce the processing burden, the differential detection approach offered by CATSI measures the IR radiation from a target scene which is optically combined onto a single detector out-of-phase with the IR radiation from a corresponding background scene, resulting in the target signature being detected in real-time void of significant background clutter. During the past ten years, the sensitivity and accuracy of the differential detection approach with the CATSI sensor has been well established at several field trials. This work includes a major U.S. open-air field trial in Nevada (2001) for a standoff distance of 1.5 km (Fig. 2), and a trial at DRDC Valcartier for a standoff distance of 5.7 km (Fig. 3) [4,5]. All of these experiments clearly demonstrate the outstanding capability of the technique (CATSI and GASEM) for on-line monitoring and surveillance.

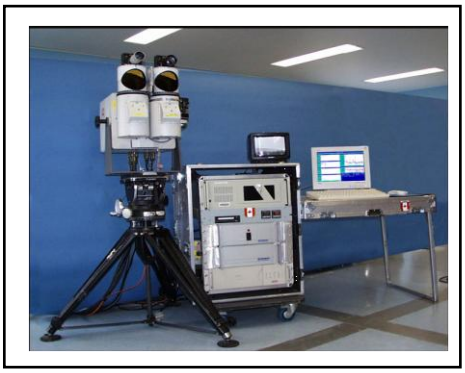

Figure 1: Photograph of the CATSI instrument mounted on a tripod.

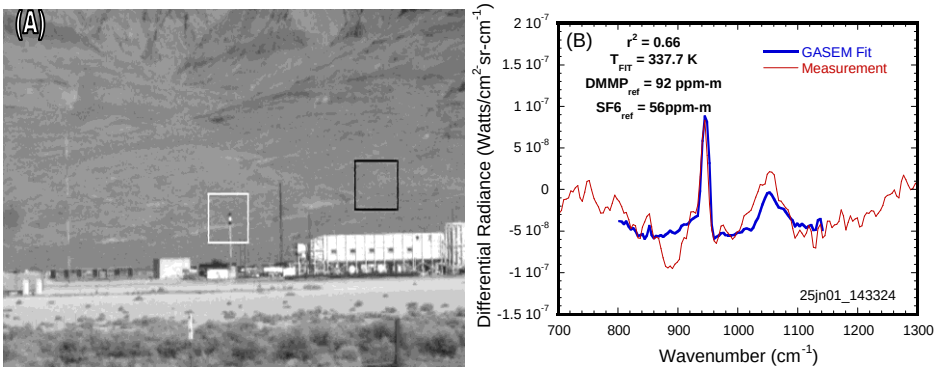

Figure 2: (A) Photograph of the 1.5-km medium range test site at Nevada. (B) Detection and identification of DMMP and SF_6 in a gas mixture at a distance of 1.5 km.

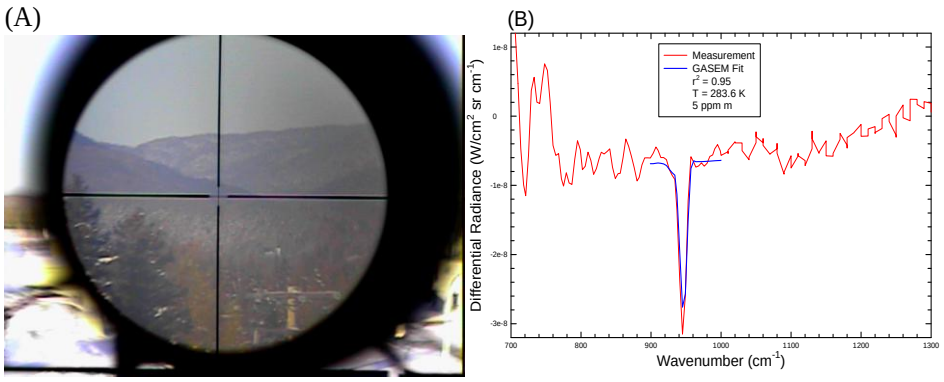

Figure 3: (A) View of the 5.7-km long path facing towards the laboratory that contains the source. (B) Detection and identification of SF_6 at a distance of 5.7 km from the CATSI receiver.

1.2 MoDDIFS Sensor Project

The success of the CATSI system for detecting chemical vapours has led to the development of a novel R&D prototype, MoDDIFS (Multi-Option Differential and Imaging Fourier Spectrometer), to address the standoff detection of explosives and explosive precursors [6]. The MoDDIFS system will provide a differential imaging capability that may be very useful for the passive standoff detection of vapours from particular explosives and precursors. To detect such materials emanating from a building or any location under surveillance can provide early detection and warning of a belligerent's intent and their level of readiness to mount an attack with improvised explosives. The sensor will be optimized for explosives and precursor detection based on phenomenological and modeling studies and a new library of relevant explosive and precursor signatures. MoDDIFS is a R&D project sponsored by the Canadian CBRNE Research and Technology Initiative (CRTI) program.

1.3 List of Explosives and Precursors

Certain explosives and chemical precursors are more amenable to detection by a MoDDIFS-type sensor due to their relatively high vapour pressure and the presence of an IR signature. A preliminary list of relevant explosives and precursor chemicals and some sample signatures measured at DRDC Valcartier is presented in Table 1 and Fig. 4, respectively. The existence of spectral signatures is the basis upon which standoff detection is made possible.

Table 1 : Detectable Explosives and Precursors

Compounds	Material Class	Detectable Phase	Potential Detection	Detection Scenarios	Spectral Signature
TATP	Explosive	Vapor/Solid	YES*	Leak/Spill	YES
HMTD	Explosive	Vapor/Solid	MAYBE #	Leak/Spill	To be measured
NG	Explosive	Vapor/Liquid	MAYBE #	Leak/Spill	To be measured
EGDN	Explosive	Vapor/Liquid	MAYBE #	Leak/Spill	To be measured
RDX	Explosive	Solid	YES*	Spill	YES
PETN	Explosive	Solid	YES*	Spill	YES
AN-FO	Explosive	Solid	?	Spill	To be measured
Chlorates**	Explosive	Solid	MAYBE*	Spill	YES
Nitric acid	Precursor	Vapor/Liquid	YES*	Leak/Spill	YES
Hydrogen peroxide	Precursor	Vapor/Liquid	YES*	Leak/Spill	YES
Acetone	Precursor	Vapor	YES*	Leak/Spill	YES
Hexamine	Precursor	Powder	LIKELY*	Leak/Spill	YES

* If sufficient concentration; # If spectral signature exists; ** for e.g., potassium chlorate (other chlorates/perchlorates will be similar)

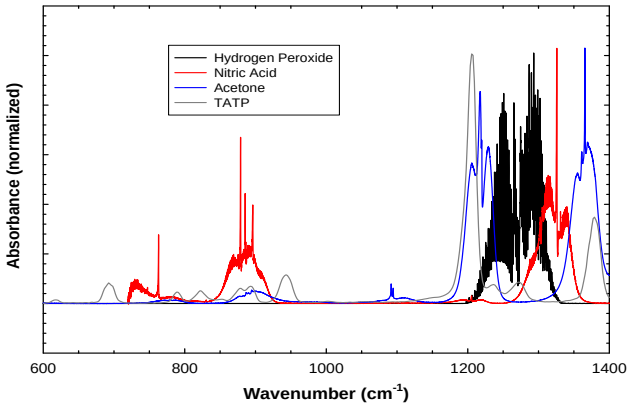

Figure 4: Absorbance spectra for vapours of important explosives and precursors.

1.4 Detection of Explosive Vapours and Precursors

The methodology we propose combines the clutter suppression efficiency of the differential detection approach with the high spatial resolution provided by the hyperspectral imaging approach. This will consist of integrating an imaging capability of the advanced IR imager, Hyper-Cam (developed by Telops, Inc) with a differential CATSI-type sensor. A schematic presented in Fig. 5 summarizes the advantage gained by adding an imaging capability to CATSI, which forms the essential basis of the new MoDDIFS sensor. The CATSI sensor is optimized for probing spatially-large chemical clouds (cloud size of 10 m at a distance of 1 km). This limit determines the size of the detector, which is 1 mm in the case of CATSI. Therefore, the CATSI performance is limited when probing a plume that is smaller than the field-of-view (FOV) of the sensor. A simple analysis based on signal-to-noise ratio (SNR) demonstrates the gain in sensitivity that can be achieved by adding a multi-pixel detector to a CATSI-like spectrometer. The SNR is an important parameter since it determines the sensitivity limit of a system. In general, spectral features of a target will be detected if they are at least three times as intense as the noise (i.e., SNR > 3). The SNR of a spectrometer having a single element detector is given by the following equation,

$$SNR = \frac{KD^2 A_{plume} B}{\sqrt{A_{\det}}}, \qquad (1)$$

where K represents the responsivity of the instrument, D is the diameter of the telescope, B is the number of photons/m^2 emitted by a plume that reaches the detector, A_{plume} is the area of the probed plume and A_{det} is the area of the detector. An important fact expressed by Eq. 1 is that the SNR is inversely proportional to the detector size (i.e., smaller detectors have higher SNR). Consequently, an FTIR imager that incorporates small pixel elements responds with higher SNR when probing small-dimension plumes [5]. This effect is summarized in Fig. 5(A,B), where the SNR of CATSI and MoDDIFS has been estimated for a typical explosive precursor scenario involving the detection of a 10-cm diameter plume of acetone at a distance of 300 m from the detector. For the CATSI sensor in Fig. 5A, the SNR estimate of 0.33 was obtained by scaling the SNR value of 10 determined from the measured spectrum of an acetone cloud in the laboratory, as shown in Fig. 5(C,D). By application of Eq. 1, the SNR corresponding to a 10-cm acetone cloud at a range of 300 m from the sensor is reduced to a value of 0.33 for a CATSI type-sensor with a 30-cm telescope and a 1 mm detector. The same measurement scenario incorporating a MoDDIFS-type sensor with a detector size of 30 microns results in an estimated SNR of 10. This estimate clearly shows that advantage in SNR to be gained in using a MoDIFFS-type sensor to detect spatially-small vapor clouds at large distances.

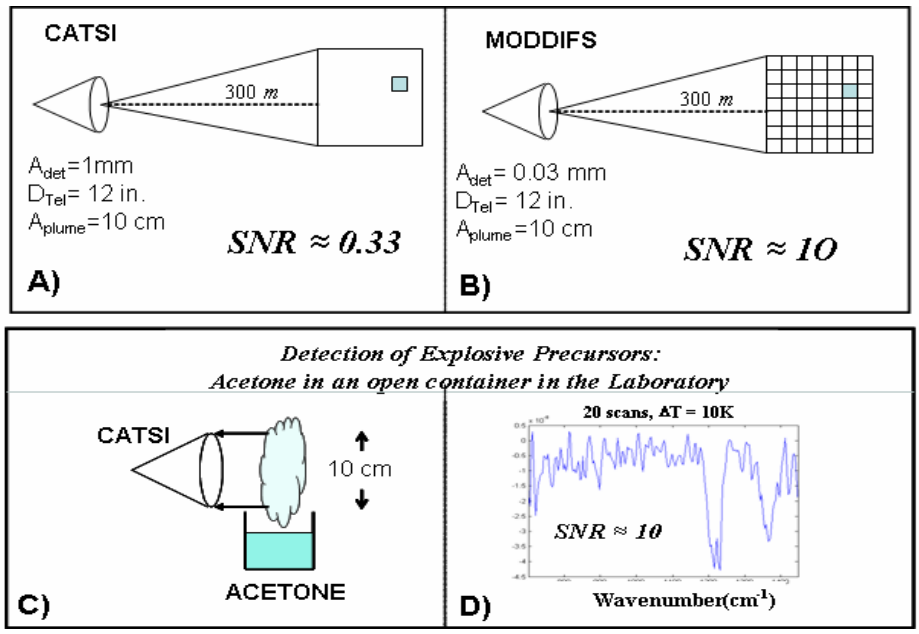

Figure 5: Evaluation of SNR for a MoDDIFS-type sensor based on SNR derived for CATSI.

1.5 Detection of Liquid and Solid Explosive Contaminants

Polarization sensing with CATSI has also been tested with promising results for the standoff detection of liquid chemical warfare surface contaminants [7]. The proposed project will see this approach extended to the standoff detection of liquid explosives and precursors. Differential polarization measurements will substantially mitigate the spectral clutter arising in the measurement due to the natural variability associated with the background sky radiance. Fig. 6 shows a diagram in which the radiance from a VX-contaminated surface is probed by a sensor having either a polarizer oriented parallel (p-polarization) or perpendicular (s-polarization) to the plane of incidence. Subtracting the two polarized radiances yields the differential polarization radiance which is strongly perturbed by the presence of VX [7]. In a recent

simulation study it has been shown that even for thick contaminant layers, the differential polarization sensing approach is sensitive enough to detect and identify the refractive index signature of air-liquid interfaces. This attribute is promising for application to the standoff detection of liquid explosives and precursor spills.

Although liquid explosives have been used only in rare occasions, the possibility of detecting explosive spills and the associated precursors remains a valuable investigative tool. Examples of liquid precursors used in HME processing include glycerin, ethylene glycol (antifreeze), nitric acid and sulfuric acid, for which spills may have the potential to be detected by standoff differential polarization sensing.

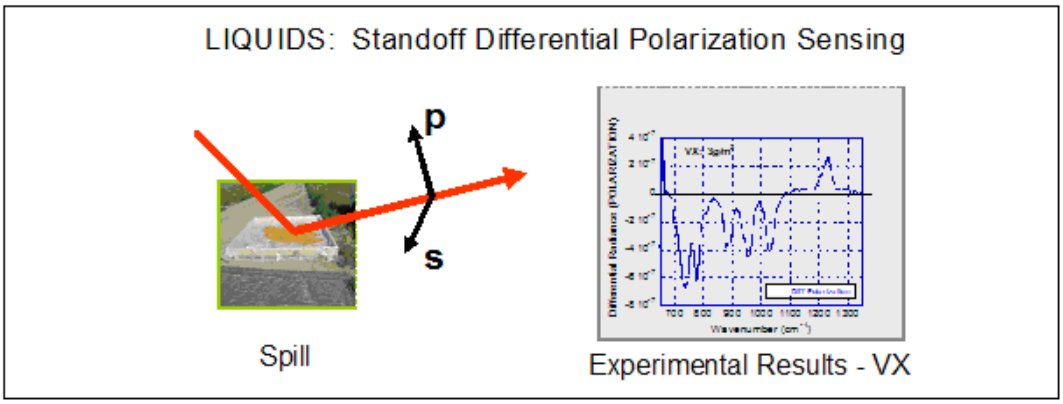

Figure 6: Differential polarization sensing scenario (left) and the resulting differential polarization spectrum showing the presence of VX

Differential polarization sensing can also be applied to the detection of explosive powders. Detection using non-polarized measurements has already been proven, as shown for the case of TNT in Fig. 7. It has been established that most explosive powders exhibit strong IR signatures [8], and the introduction of a differential polarization method should enhance the detectability of these powders.

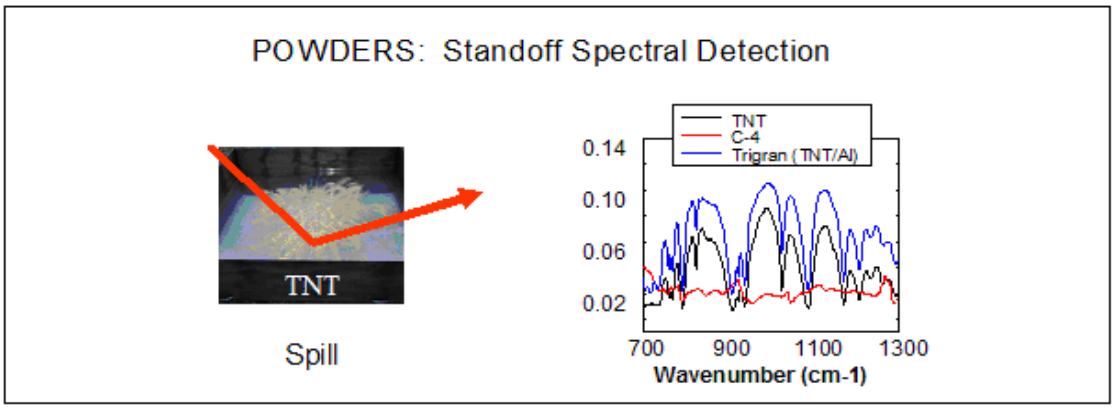

Figure 7: Current sensing scenario (left) and typical IR signatures of common explosives

PART 2: AIRBORNE HSI REMOTE SENSING ACTIVITY

2.1 Introduction

As shown in the first part of this paper, ground-based passive standoff sensors based on FTIR technology have been shown to be successful and reliable in detecting and identifying chemical threats in both vapour and solid/liquid phases. Transitioning ground-based FTIR technology to an airborne platform promises similar detection possibilities with vastly greater area coverage. To this end, DRDC Valcartier has been investigating the implementation of a commercial-off-the-shelf (COTS) hyperspectral imager for its airborne remote sensing capability. The system consists of the longwave infrared Hyper-Cam-LW imaging sensor integrated on a stabilization platform with image motion compensation (IMC) mirror and inertial navigation system – global positioning system (INS-GPS) [9]. A number of field trials were undertaken at DRDC Valcartier in the winter 2008 and spring 2009 to test the airborne Hyper-Cam's capability for detecting chemical plumes and powders.

2.2 Airborne Configuration

In the airborne configuration, shown in Fig. 8, the Hyper-Cam stares at a constant scene through the application of an image compensation mirror, as shown in Fig. 9, to account for the pitch, roll and the forward motion of the aircraft [9].

Figure 8: Illustration of the airborne configuration with two Hyper-Cams (Courtesy of Telops, Inc)

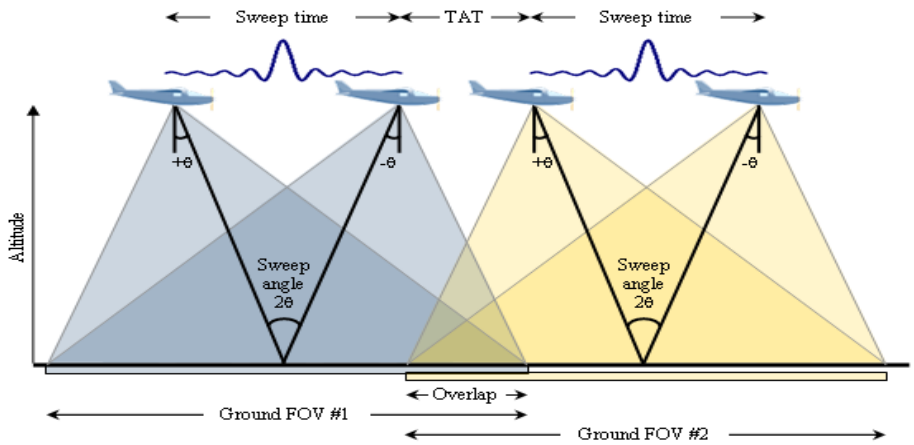

Figure 9: Interferogram acquisition in airborne configuration (Courtesy of Telops, Inc)

2.3 Airborne Hyper-Cam Experiments

Three experiments were set up at DRDC Valcartier to test the Hyper-Cam's capability for detecting gas plumes and chemical powders, along with a number of calibration panels to help quantify the noise equivalent spectral radiance (NESR) and sensor pointing stability. The three DRDC experiments were carried out on December 19, 2008, March 5, 2009 and April 30, 2009. In the case of the first two experiments, overcast cloud cover formed by the time the aircraft was ready to acquire data; however, mostly clear conditions prevailed for the third experiment.

The basic experimental setup used at DRDC Valcartier to perform tests on the airborne Hyper-Cam is shown in Fig. 10. On December 19, the ground targets consisted of 2m×2m black and reflective panels, a portable plume generator capable of emitting SF6 gas at a maximum rate of 100 L/min, a 2m×2m thin plastic sheet of polypropylene (to act as a stable plastic 'plume'), and a 2m×2m wooden tray of ammonium sulphate fertilizer. Photographs of several of the targets in the winter conditions are shown in Fig. 11. It is apparent that the sky conditions were favourable during the set up of the experiment; unfortunately, overcast cloud formed later during the airborne collection period. Four passes of the airborne Hyper-Cam-LW were made over the DRDC experiment. For the April 30 experiment, Freon-134a was added as an additional gas release.

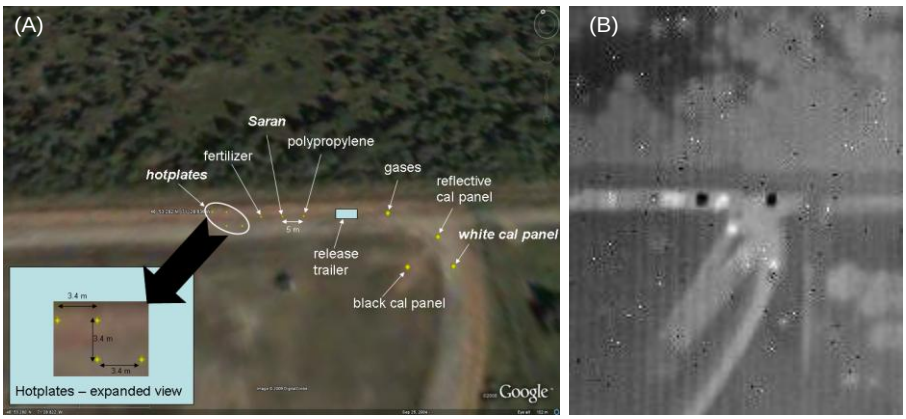

Figure 10: (A) Google Earth image of the experimental setup used to test the Hyper-Cam sensors in an airborne configuration. During the first two experiments the background actually consisted of snow.

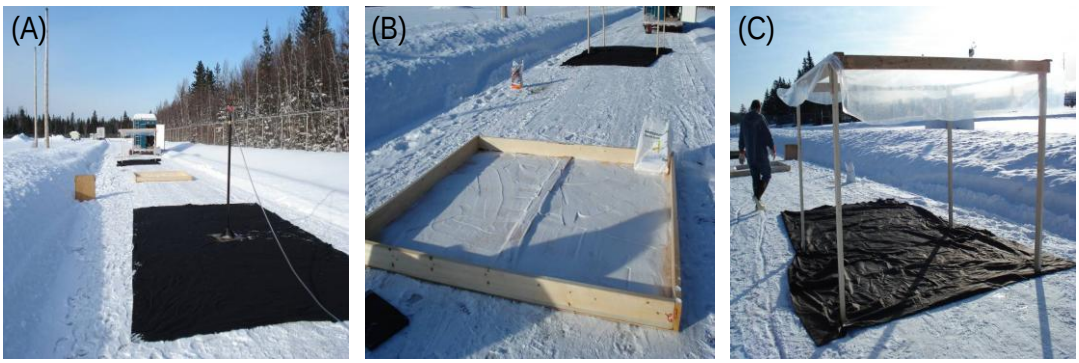

Figure 11: Experimental targets set up for the airborne Hyper-Cam collect, including (A) SF_6 gas plumes with a black background to enhance the temperature contrast, (B) ammonium sulphate fertilizer, and (C) polypropylene plastic with a black background.

2.4 Test Results and Discussion

The Generalized Likelihood Ratio Test (GLRT) was the detection algorithm used to identify gas plumes and other chemical targets in the experiment. This test has been used extensively by DRDC in previous work, and a detailed description of the method is given in reference [10,11]. Essentially, the GLRT is described mathematically by:

$$\text{GLRT:} \qquad \frac{m^T P_B^{\perp} m}{m^T P_{BS}^{\perp} m} = \frac{\left(P_B^{\perp} m\right)^T \left(P_B^{\perp} m\right)}{\left(P_{BS}^{\perp} m\right)^T \left(P_{BS}^{\perp} m\right)} = \frac{\left\| P_B^{\perp} m \right\|^2}{\left\| P_{BS}^{\perp} m \right\|^2}$$

Where the numerator represents the squared norm of the measurement, m, projected out of the background space, B, and the denominator represents the squared norm of the measurement projected out of the background plus signature space, S. If the measurement does not contain the signature of interest, the result of the GLRT is approximately one.

The detection and identification of SF6 gas during a release at 100 L/min is shown in Figs. 12A-C. The upper panel in Fig. 12A shows the measured calibrated radiance spectrum (blue curve) and the SF6 reference absorbance spectrum (green curve). The result of projecting the measurement out of the background space is shown by the blue curve in the lower panel of Fig. 12A. This is compared to the projection of the signature out of the background shown by the green curve. The absorption feature of SF6 is apparent at 950 cm-1. The output of the GLRT filter is summarized in Fig. 12B, which shows the detection of SF6 above the threshold level, which was set at ten times the root-mean-square (rms) value of the background result. The detection and identification of a small SF6 plume in the scene image is shown in the upper panel of Fig. 12C. The lower panel shows the complete detection result.

A simple band ratio method was also used to detect the SF6 gas. Figure 13A represents the LWIR image measured by the airborne Hyper-Cam and the location of the gas release. Figure 13B shows the result of taking the ratio of the SF6 absorption band at 950 cm^{-1} and the 970 cm-1 band, which was representative of the background only. The SF6 absorption feature is clearly evident only in the location of the gas release point, similar to the GLRT result in Fig. 12C.

It should be noted that the environmental conditions for detection were poor. By the time the measurements were underway, overcast clouds had moved in to reduce the temperature contrast between the gas and background scene, thus reducing the ability to detect the gas.

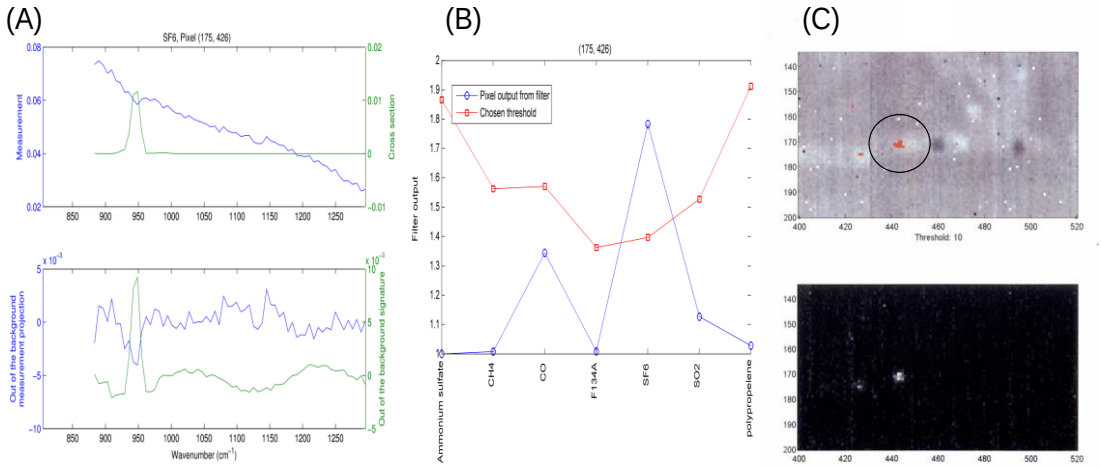

Figure 12: The detection and identification of SF_6 gas using the GLRT algorithm. The figures are explained in the text.

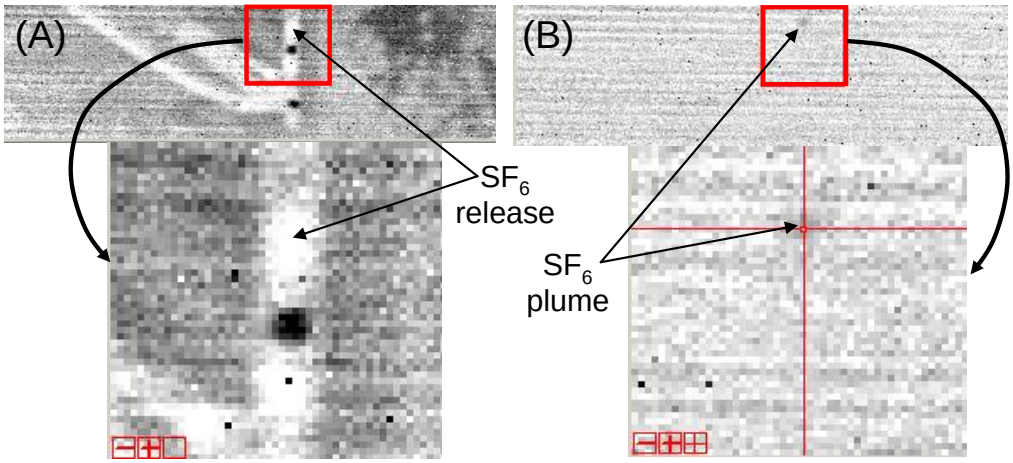

Figure 13: Detection of SF_6 plume based on the ratio of two bands; one at 950 cm^{-1} where SF_6 absorbs energy and one at 970 cm^{-1} where no absorption occurs. The measured radiance is shown in (A) and the band ratio in (B).

The detection and identification of F-134a during a release at 100 L/min on April 30 is shown in Figs. 14A-C. The upper panel in Fig. 14A shows the measured calibrated radiance spectrum (blue curve) and the F-134a reference absorbance spectrum (green curve). The result of projecting the measurement out of the background space is shown by the blue curve in the lower panel of Fig. 14A. This is compared to the projection of the signature out of the background shown by the green curve. The output of the GLRT filter is summarized in Fig. 14B, which shows the detection of F-134a above the threshold level, which was set at ten times the root-mean-square (rms) value of the background result. The detection and identification of the F-134a plume in the scene image is shown in Fig. 14C.

The detection and identification of ammonium sulphate fertilizer on April 30 is shown in Figs. 15A-C. The upper panel in Figure 15A shows the measured calibrated radiance spectrum (blue curve) and the ammonium sulphate reflectance spectrum (green curve). The result of projecting the measurement out of the background space is shown by the blue curve in the lower panel of Figure 15A. This is compared to the projection of the signature out of the background shown by the green curve. The output of the GLRT filter is summarized in Figure 15B, which shows the detection of ammonium sulphate above the threshold level, which was set at ten times the root-mean-square (rms) value of the background result. The detection and identification of the ammonium sulphate fertilizer in the scene image is shown in Figure 15C.

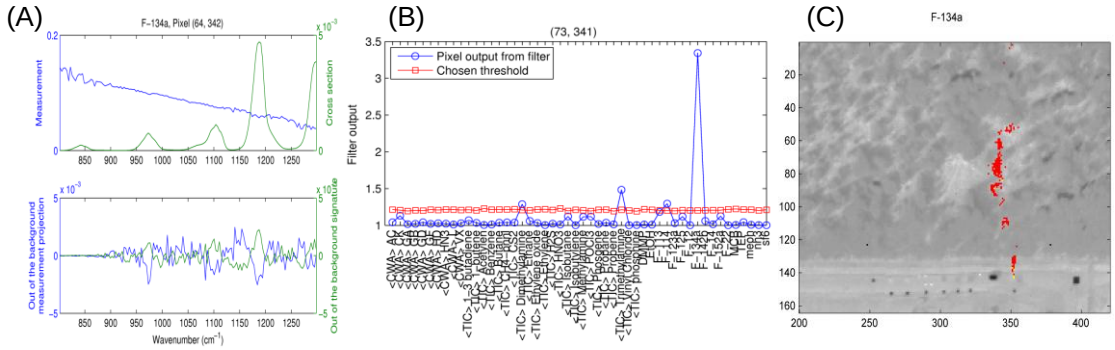

Figure 14 : The detection and identification of F-134a gas using the GLRT algorithm. The figures are explained in the text.

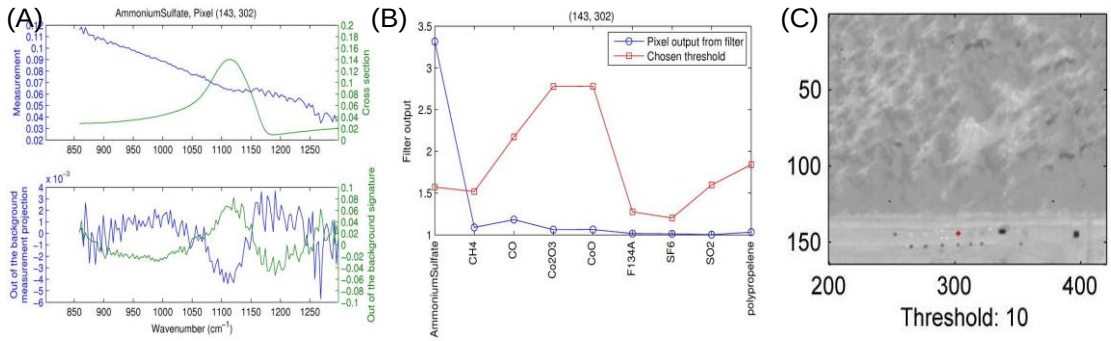

Figure 15: The detection and identification of ammonium sulphate fertilizer using the GLRT algorithm. The figures are explained in the text.

2.5 NESR and Calibration

Several targets were used to help characterize the quality of the radiometric calibration and to make a preliminary determination of the average NESR of the Hyper-Cam-LW system across the 8 – 11 micron band. The scene used for this investigation, as shown in Fig. 16A, consisted of measurements from a reflective (cold) sheet of sandblasted aluminum (Fig. 16B), a sheet of sandblasted aluminum covered with Aeroglaze paint (Fig. 16C) and the snow itself (Figure 16D), which behaves approximately like a blackbody in the LWIR region. Fig. 16E shows the spectral measurements in terms of equivalent brightness temperature for each of these targets. Each target produced approximately 6 pixels of pure signal, as included in Fig. 16E. One common characteristic among the lower three curves is the apparent increase in temperature as a function of wavenumber. All three curves were measured in the same pass using the same calibration scheme. The uppermost curve was measured during a different pass, and it is noticeably more uniform than the other curves. It, therefore, appears that an anomaly exits in the calibration process, and this is currently under investigation. The brightness corresponding to the reflective target shows a feature in the 1000 – 1100 cm-1 region, which is most likely attributable to atmospheric ozone, despite the presence of the overcast cloud layer.

The uppermost curve (offset by +15K) corresponding to the blackbody target represented a brightness temperature of 265 +/- 0.5 K (rms) in the 900 – 1000 cm-1 region. This compared well with a ground-based measurement of 264.7 K, measured with a high accuracy hand-held infrared camera. The rms error of 0.5 K for one spectral measurement provides a preliminary estimate of the average noise equivalent delta temperature (NEDT) of the Hyper-Cam system. This translates into an NESR value of about 5×10-8 W/cm^2 sr cm^{-1} (or 5 μflicks) at 1000 cm-1 for a spectral resolution of 6 cm-1 (FWHM).

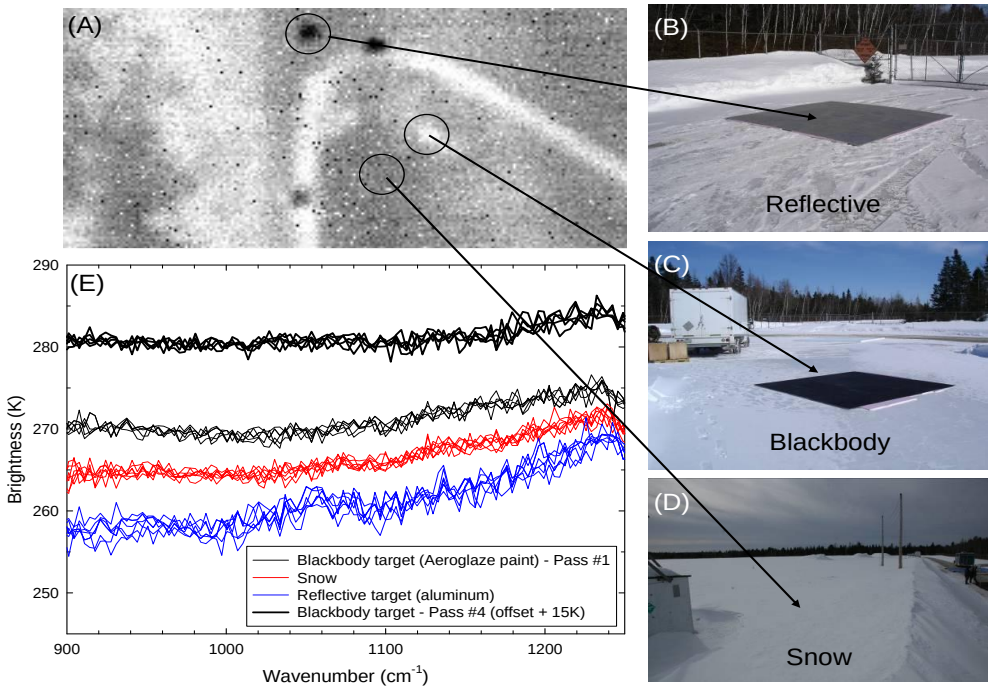

Figure 16: (A) Measured LWIR Hyper-Cam image showing (E) the spectral brightness temperatures of (B) a reflective target, (C) a blackbody, and (C) snow.

3. CONCLUSIONS

Passive FTIR detection technologies have matured to a point where detector sensitivity, detection algorithms and phenomenology understanding appear now ready for application to the standoff detection of explosive materials. In particular, the unique differential sensing capability of the CATSI system has been well validated for chemical vapour detection at distances greater that 5 km. It is clear that this differential capability can be applied to the standoff detection of relevant explosives and their precursors. This can be realized through the development of a highly specialized differential imager, MoDIFFS, which will be optimized for the standoff detection of explosives and explosive precursors.

The current mature state of ground-based standoff FTIR technology now makes it worthwhile to also investigate its capacity from an airborne platform. A COTS hyperspectral system, the Hyper-Cam-LW FTIR imager, has been recently installed by Telops, Inc on an aircraft platform consisting of a stabilization module, IMC mirror and INS/GPS system.

Three experiments were performed at DRDC Valcartier to investigate the performance of the airborne Hyper-Cam system. These experiments included chemical vapour releases and chemical powders, such as fertilizer. Exploitation of the hyperspectral images indicates it is possible to correctly detect and identify the chemical targets under varying atmospheric conditions. A preliminary estimate of the average NESR of the airborne Hyper-Cam sensor across the 800 – 1200 cm^{-1} band was determined to be about 5×10^{-8} W/cm^2 sr cm^{-1} (or 5 μflicks or 0.5 K at 1000 cm^{-1}).

REFERENCES

[1] J.-M. Thériault, IR Fourier Spectrometer for Differential Detection: Design, Prototype and Results, DREV R-9804 (1998).

[2] J.-M. Thériault, Modeling the responsivity and the Self-emission of a Double-beam Fourier-transform Infrared Interferometer, Appl. Opt., **38**, No. 3, pp. 505-515 (1999).

[3] J.-M. Thériault, Passive Standoff Detection of Chemical Vapors by Differential FTIR Radiometry, DREV-TR-2000-156, 76 pages (2001).

[4] J.-M. Thériault, E. Puckrin, F. Bouffard and B. Déry, Passive Remote Monitoring of Chemical Vapors by Differential FTIR Radiometry: Results at a Range of 1.5 km, Appl. Opt., **43**, 1425-1434 (2004).

[5] H. Lavoie, E. Puckrin, J.-M. Thériault and F. Bouffard, Passive Standoff Detection of SF6 at a Distance of 5.7 km by Differential FTIR Radiometry, Appl. Spectrosc., **59,** 1189-1193, (2005).

[6] J. -M. Thériault, E. Puckrin, H. Lavoie, F. Bouffard, S. Désilets, and P. Caron, CRTI Project: Explosive Vapors Standoff Detector – Multi-Option Differential Detection and Imaging Fourier Spectrometer (MoDDIFS), Public Security S&T Summer Symposium 2009, Ottawa, Canada, June 16-18, (2009).

[7] J. -M. Thériault, H. Lavoie, E. Puckrin, and F. Bouffard, Passive standoff detection of surface contaminants: A novel approach by differential polarization FTIR spectroscopy, Special Issue: IJHSES- International Journal of High Speed Electronics and Systems, **18**, 251-262 (2008).

[8] E. Puckrin, J.-M. Theriault, H. Lavoie, D. Dubé and P. Brousseau, Novel application of passive standoff radiometry for measurement of explosives, Special Issue: IJHSES- International Journal of High Speed Electronics and Systems, **18**, 307-318 (2008).

[9] J. Allard, M. Chamberland, V. Farley, Airborne measurements in the longwave infrared using an imaging hyperspectral sensor, Proceedings of SPIE Vol. **7086**, 70860K (2008).

[10] M. Manolakis, D. Marden, G.A. Shaw, Hyperspectral image processing for auto-matic target detection applications, Lincoln Laboratory Journal, **14**, 79 (2003).

[11] L. Scharf, and B. Friedlander, Matched subspace detectors, IEEE Transactions on Signal Processing, **42**, 2146 (1994).